Trapping in bottlenecks: interplay between microscopic dynamics and large scale effects

Emilio N.M. Cirillo
E_mail: emilio.cirillo@uniroma1.it
Dipartimento di Scienze di Base e Applicate per l'Ingegneria, Sapienza Università di Roma, via A. Scarpa 16, I–00161, Roma, Italy.

Matteo Colangeli
Dipartimento di Ingegneria e Scienze dell'Informazione e Matematica, Università degli Studi dell'Aquila, Via Vetoio, 67100 L'Aquila, Italy.
E_mail: matteo.colangeli1@univaq.it

Adrian Muntean
Department of Mathematics and Computer Science, Karlstad University, Sweden.
E_mail: adrian.muntean@kau.se

Abstract. We investigate the appearance of trapping states in pedestrian flows through bottlenecks as a result of the interplay between the geometry of the system and the microscopic stochastic dynamics. We model the flow trough a bottleneck via a Zero Range Process on a one–dimensional periodic lattice. Particle are removed from the lattice sites with rates proportional to the local occupation numbers. The bottleneck is modelled by a particular site of the lattice whose updating rate saturates to a constant value as soon as the local occupation number exceeds a fixed threshold. We show that for any finite value of the threshold the stationary particle current saturates to the limiting bottleneck rate when the total particle density in the system exceeds a critical value corresponding to the bottleneck rate itself.

Keywords: Pedestrian flows through bottlenecks; trapping; condensation; stochastic modeling; interacting particle systems.

AMS Subject Classification: 90B06, 60K30, 82C22

1. Introduction

The effect of bottlenecks on a flow in a lane is relevant in many applied contexts such as traffic [1, 2] and pedestrian [3–7] flows, motion in biological systems [8–10], but also in more abstract problems such as the study of the effect of blockage in stationary states [11–13] or the effect of obstacles on two–dimensional particle flows [14–16].

Bottlenecks are usually the effect of a local *capacity reduction* of the lane which can be due to different reasons such as speed reduction, shrinkage of the lane, or decrease of the field governing the motion. In the case of pedestrian flows, which will be the application we shall focus on in the sequel, bottlenecks are typically due to the presence of a door or a corridor which shrinks the lane width inducing a direct capacity reduction. A huge amount of engineering research is ongoing on questions like crowd evacuation, route choices, doors design and results are mostly experimental, often not conclusive [17,18]. A general agreement is lacking. As regards the interplay between flow dynamics and door geometry, we discover that general laws govern the structure of fundamental diagrams, and point out the presence of trapping (condensation) regimes. Interestingly, we shed also light on parameter regimes that prevent the onset of those trapping states. Our findings, see Section 4, are thus expected to have a relevant impact on crowd management and building design, especially when big perturbations, e.g. due to fire, accidents, terrorist attacks, potentially occur in the flow of pedestrians. In particular, we get a precise understanding of how the door size affects the structure of the fundamental diagrams, see Fig. 4.5.

Usually the motion is affected by the reduced capacity of the lane only if the local density is sufficiently large, that is, namely, if the number of pedestrians moving through the reduced capacity region is high. Think, for instance, to pedestrians walking through a door: if the number of people approaching the door per unit of time is low, such a capacity reduction will have no effect on the flow. On the other hand, if the approaching rate is high enough, pedestrians will be not able to pass through the door efficiently and the total flux will hence decrease. In other words, in these situations the capacity reduction will affect the flow only if the local density overcomes a certain *saturation threshold*.

Thus, this blockage phenomenon depends essentially on two parameters: the saturation threshold and the reduced capacity. We shall develop a basic model to study this problem and, in this framework, we shall explain which of the two parameters actually controls the onset of the bottleneck.

We shall consider a one–dimensional asymmetric Zero Range Process (ZRP) on the periodic lattice with updating rates proportional to the number of particles at each site, excepting on one *defect site*, modelling the reduced capacity portion of the lane, where the updating rate saturates to a value, called the *saturated rate*, when the number of particles exceeds a value, called the *saturation threshold*. When a site is updated a particle is moved forward or backward with a prescribed probability. For the Zero Range models the idea of activation and saturation thresholds was introduced in [19, 20], where different interpretations, ranging from pedestrian dynamics to the thermodynamic theory of phase transitions, have been considered. We also mention that, in the recent literature, ZRP with modified blockage rules

have also been studied in different frameworks, e.g. non–Markovian processes and traffic models [21–24].

This model can be thought of as a basic model for pedestrians on a lane with a width shrinkage due to a corridor or a door. The lane is partitioned in squared cells, each cell is a site of the ZRP model and the defect site models the cell where the blockage takes place, see Fig. 1.1. The number of particles at a site is the number of pedestrians in the corresponding cell. Pedestrians moving in a given direction can be modelled by assuming that the particles can only jump forward (or, equivalently, backward). Pedestrians that can move back and forth on the lane can be modelled by assuming that the probabilities for a particle to move backward or forward on the lattice are both different from zero. Using a stochastic model, rather than a deterministic one, allows to take into account the effects of density fluctuations in the pedestrian flow (real walkers do not move all at the same instant). As it will be explained in the following section, these fluctuations seem to induce a reduced flow even in a setup in which the total pedestrian density on the lane would not justify it.

By exploiting the theory of condensation for ZRP [25–29] we shall prove that, in such a setup, the parameter controlling the onset of the bottleneck mechanism is the saturated rate. More precisely, we shall see that, provided the total density of the system is large with respect to the saturated rate, the system exhibits a condensed state characterized by a reduced flow proportional to the saturated rate. It is worth noting that the model studied in this paper is an example of ZRP with updating rates not decreasing with the number of particles and exhibiting a condensed state induced by a local inhomogeneity in the updating rates. Our model should be compared with the one studied in [26, Section 5.2] where all the site updating rates are set equal to one except for one site which is updated at a lower constant rate. This peculiar behavior at one site is sufficient for the condensed state to appear, provided that the total density is large enough with respect to the lowered updating rate. In our model, on the contrary, the updating rate is proportional to the local occupation number for any site except on the defect site, where it saturates to a constant value (possibly even much larger than one!). In the sequel we shall then prove that also this updating mechanism may lead to condensation, provided the total density is large enough with respect to the saturated constant rate.

This result, in terms of the pedestrian interpretation, can be rephrased as follows. The pedestrian current is decreased by the capacity reduction on the lane if pedestrian total density is large compared to the saturated rate which pedestrians experience in the region of the lane with capacity reduction. Moreover, in this regime the pedestrian flux is proportional to the saturated rate, which, in the case of a capacity reduction caused by the presence of a door, it is reasonable to assume to be proportional to the door width. Note that this

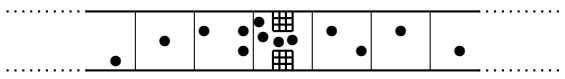

Figure 1.1: Sketch of pedestrians moving on the lane. The cell at the center is the one in which walkers experience the blockage and corresponds to defect site of the lattice model. In the lattice model each cell is lumped to a single site.

result is indeed found in different experimental setups [2, 3]. We shall also unravel the main features of the fundamental diagram associated to our model, in which we plot the local speed as a function of the local particle concentration. In particular, we find results showing striking agreement with a set of experimental data measured in a situation similar to the one considered in our abstract setup [30].

The paper is organized as follows. In Section 2 we define the model and discuss the results. Section 3 is devoted to the analytical study of the model. In Section 4 we discuss our results in view of the pedestrian flow interpretation of the model.

2. Model and results

To define the ZRP to be studied in this paper we borrow the notation from [26]. We consider the positive integers L, N, the finite torus $\Lambda = \{1, \dots, L\}$, and the finite *state* or *configuration space* $\Omega_{L,N}$ made of the states $n = (n_1, \dots, n_L) \in \{0, \dots, N\}^\Lambda$ such that $\sum_{x=1}^{L} n_x = N$. Given $n \in \Omega_{L,N}$ the integer n_x is called *number of particle* at site $x \in \Lambda$ in the *state* or *configuration* n. The integer $1 \le T \le N$ and the real $c > 0$ are respectively called *saturation threshold* and *saturated rate*. For any site $x \in \Lambda$, the hopping rate $u_x : \mathbb{N} \to \mathbb{R}_+$ is defined as follows: $u_x(0) = 0$ for $x = 1, \dots, L$, $u_1(k) = k$ for $1 \le k \le T$ and $u_1(k) = c$ for $T + 1 \le k \le N$, and $u_x(k) = k$ for $x = 2, \dots, L$ and $1 \le k \le N$. The ZRP considered in this context is the continuous time Markov process $n(t) \in \Omega_{L,N}$, $t \ge 0$, such that each site x is updated with rate $u_x(n_x(t))$ and, once a site x is chosen, a particle is moved to the neighboring site $x + 1$ with *forward hopping probability* $1/2 < p \le 1$ and to the neighboring site $x - 1$ with probability $0 \le 1 - p < 1/2$ (recall that periodic boundary conditions are imposed). Note also that when $T = N$ the model is equivalent to independent particles random walk.

In words the dynamics can be described as follows: any site is updated at a rate which is a function of the number of particles occupying that particular site. For all the sites, but a defect one, the rate increases linearly with the number of particles occupying the site. At the defect site, the rate increases linearly with the number of particles at that site from zero to

an a priori fixed threshold value T; when the number of particles at the defect site is larger than T the rate is equal to a constat value c. Once a site is selected, a particle is removed from that site and displaced one site forward with probability p or one site backward with probability $1-p$. As mentioned in the Introduction, this simple model can be thought as a basic model for pedestrian motion on a lane: the lane is made of square cells and each cell is lumped to a site of the ZRP model. The number of particles at a site is the number of pedestrians in the corresponding cell in the lane. The fact that pedestrians can move back and forth is modelled by assuming that the forward jump probability p is different from 0 and 1. If one assumes $p = 0$ (resp. $p = 1$) a backward (resp. forward) pedestrian flow is modelled.

It can be proven, see e.g. [26, equations (2) and (15)], that the *invariant* or *stationary measure* of the ZRP process is

$$\mu_{L,N}(n) = \frac{1}{Z_{L,N}} \prod_{\substack{x=1,\dots,L:\\ n_x\neq 0}} \frac{1}{u_x(1)\cdots u_x(n_x)} \tag{2.1}$$

for any $n \in \Omega_{L,N}$, where the *partition function* $Z_{L,N}$ is the normalization constant

$$Z_{L,N} = \sum_{n\in\Omega_{L,N}} \prod_{\substack{x=1,\dots,L:\\ n_x\neq 0}} \frac{1}{u_x(1)\cdots u_x(n_x)} \ . \tag{2.2}$$

The *stationary current* $J_{L,N}$ represents the average number of particles crossing a bond between two given sites in unit time and is defined by $\mu_{L,N}[pu_x - (1-p)u_{x+1}]$. Since periodic boundary conditions are imposed, the current does not depend on the chosen bond and is given by

$$J_{L,N} = (2p-1)\mu_{L,N}[u_x] \ . \tag{2.3}$$

Other relevant quantities are the stationary mean occupation numbers given by $m_{x,L,N} = \sum_{n\in\Omega_{L,N}} n_x \mu_{L,N}(n_x)$, for any $x = 1,\dots,L$, and the stationary *particle fraction* at the defect site $\nu_{L,N} = m_{1,L,N}/N$.

The main results discussed in the sequel will be deduced in the thermodynamic limit $N, L \to \infty$, with $N/L = \rho$ being the *total constant density*. When discussing the thermodynamic limit, we shall drop the subscripts L and N from the notation and write J, m_x, and ν for the stationary current, the mean occupation number, and the particle fraction at site 1, respectively.

In the next section we show that both the particle fraction (at the defect site) and the stationary current suddenly change when the total density crosses the line $\rho = c$. In particular, the particle fraction at the defect site is zero for $\rho < c$ and positive for $\rho > c$;

	J	m_1	ν	m_x, $x \neq 1$
$\rho < c$	$(2p-1)\rho$	ρ	0	ρ
$\rho > c$	$(2p-1)c$	$\overset{L\to\infty}{\sim} (\rho - c)L + c$	$(\rho - c)/\rho$	c

Table 2.1: Stationary current, mean occupation number at the defect site, particle fraction at the defect site, and mean occupation number at the regular sites in the fluid ($\rho < c$) and condensed ($\rho > c$) state in the thermodynamic limit. For m_1 in the condensed state the large L behavior is reported.

thus, the stationary states for $\rho < c$ and $\rho > c$ are respectively called *fluid* and *condensed*. Detailed results are listed in Table 2.1.

In the fluid state particles are distributed uniformly throughout the system with mean occupation number ρ. Since $\rho < c$, sites are typically updated with rate ρ and, consequently, the current is equal to $(2p-1)\rho$. In the condensed state, instead, the occupation number at the defect site is proportional to N, hence, for L sufficiently large, it will exceed the saturation threshold T. We then have that the rate at which particles depart from such a site is c: this explain the value $(2p-1)c$ for the current. Moreover, since the current must be the same throughout the system, the rates at which the regular sites are updated attain the same value c. This explains why the mean occupation number at the regular sites is equal to c.

Analytical results are plotted in figures 2.2–2.4 together with the results of Monte Carlo simulations performed as follows: call $n(t)$ the configuration at time t, (i) a number τ is picked up at random with exponential distribution of parameter $\sum_{x=1}^{L} u_x(n_x(t))$ and time is update to $t + \tau$, (ii) a site is chosen at random on the lattice with probability $u_x(n_x(t))/\sum_{x=1}^{L} u_x(n_x(t))$, and (iii) a particle is then moved from that site to the neighboring site on the right. The results shown in the figures reveal a very good match between the analytical prediction and the numerical measures, moreover, the agreement improves when the lattice size L increases.

The Monte Carlo methods, introduced much before the invention of computers, have been one of the techniques which have supported the explosion of Statistical Mechanics in the last century. We refer to [32, Section 1.4] for a nice brief historical review. The Monte Carlo we performed follows a very classical scheme, similar to the one adopted in equilibrium Statistical Mechanics simulations, indeed, we simply realize the dynamics of the process and compute averages at stationarity. Monte Carlo techniques have been proven to be very powerful in many other fields, different from Statistical Mechanics, such as in Kinetic Theory [33]. It is worth mentioning that in this context recently very interesting

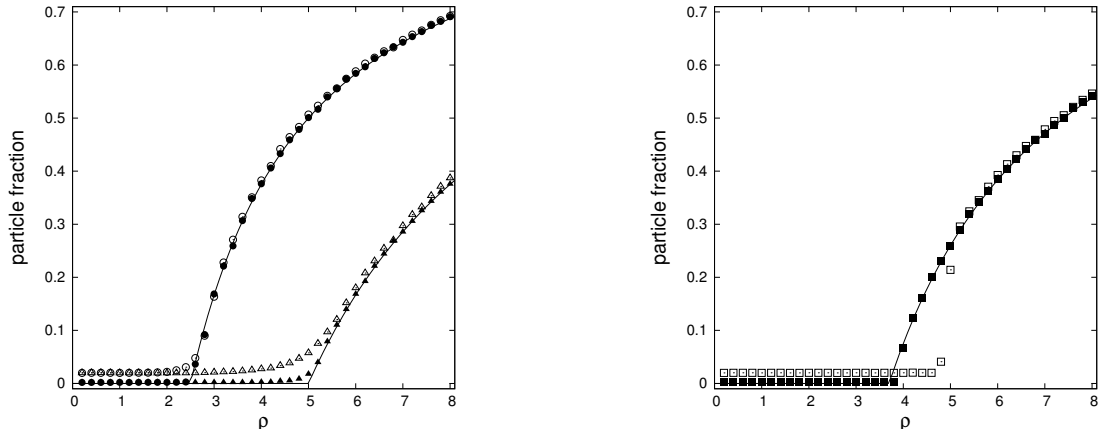

Figure 2.2: Stationary particle fraction ν (at the defect site) vs. ρ. Open and solid symbols are the Monte Carlo prediction for $L = 50$ and $L = 500$, respectively. The forward hopping probability is $p = 1$. In the left panel, circles and triangles refer, respectively, to $T = 6$ and $c = 2.5$ ($\circ$ and $\bullet$) and $T = 3$ and $c = 5$ ($\triangle$ and $\blacktriangle$). In the right panel, squares refer to $T = 15$ and $c = 3.7$ (right panel). The solid lines are the theoretical predictions given in Table 2.1.

new approaches (extension of the classical direct simulation Monte Carlo scheme) have been developed [34].

Figures 2.2 and 2.3 show Monte Carlo and analytical results when the saturation threshold and the saturated rate are kept fixed whereas the total density is varied from 0.2 to 8. Three cases are considered, namely, $T = 3$, $c = 5$, and $p = 1$ (triangles), $T = 6$, $c = 2.5$, and $p = 1$ (circles), and $T = 15$, $c = 3.7$, and $p = 1$ (squares). Results show neatly that the system remains in the fluid state until the total density exceeds the saturated rate c. Indeed, at $\rho = c$ the particle fraction, equal to zero in the fluid state, starts to increase. Note that simulations were stopped at $\rho = 8$; a further increase in ρ would correspond to a particle fraction at the defect site saturating to one. The current in the fluid state increases linearly with ρ, as ρ is the average updating rate throughout the system. On the other hand, it is constantly equal to the saturated rate c in the condensed state.

For $L = 500$ the match between the numerical measurement and the analytical computation, which holds in the thermodynamic limit, is striking. At $L = 50$, instead, finite size effects are visible. In particular, note that in the case with large threshold, i.e. $T = 15$, the stationary state switches from the fluid to the condensed phase when the total density overcomes the value corresponding to $c = 3.7$. On the other hand, when $L = 50$ the stationary state persists in the "wrong" fluid phase until the total density reaches approximately the value $\rho = 5$, cf. the right panel of Fig. 2.2. This effect can be explained as follows: in Section 3 we shall see that the two stationary states are associated with two minima of the function $I(k)$ introduced below equation (3.12). At finite volume the function I exhibits two

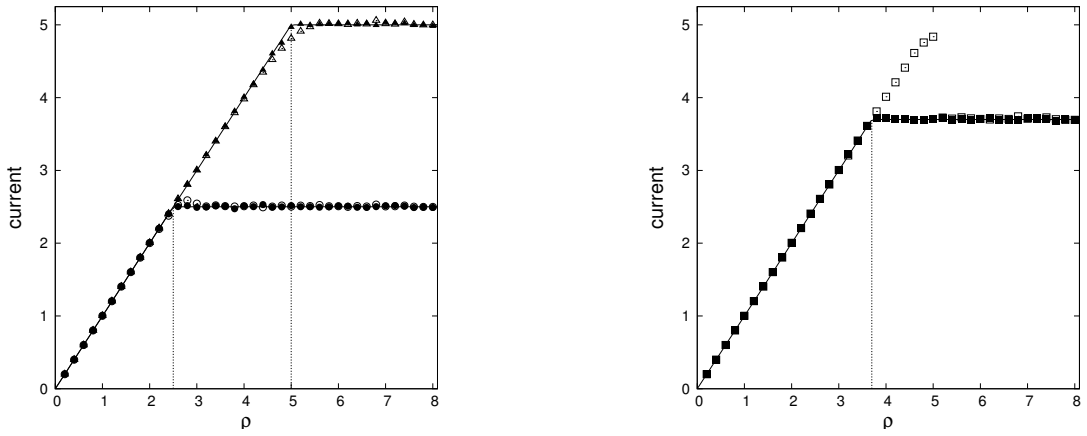

Figure 2.3: Stationary current vs. ρ. Symbols are as in Fig. 2.2. Dotted lines indicate, respectively, the values of the total density corresponding to the saturated rate $c = 2.5$ and $c = 5.0$ (left panel) and $c = 3.7$ (right panel).

minima, whereas in the thermodynamic limit only one of the two minima survives. Moreover, in the particular case shown in the picture, at $L = 50$, the wrong fluid minimum is deeper than the one corresponding to the condensed one: for this reason, the systems appears to be trapped in the fluid state. This effect is no longer visible for small values of the threshold, cf. the data referring to the cases $T = 3$ and $T = 6$.

Figure 2.4 shows Monte Carlo and analytical results when the saturation threshold and the total density are kept fixed whereas the saturated rated is varied from 0.2 to 8. Two cases are considered, namely, $T = 7$, $\rho = 2.2$, and $p = 1$ (squares) and $T = 3$, $\rho = 4.5$, and $p = 1$ (circles). Results show neatly that the system remains in the condensed state until the saturated rate c exceeds the total density ρ. Indeed, at $c = \rho$ the particle fraction, linearly decreasing with c in the condensed state, becomes constantly equal to zero. The current in the condensed state increases linearly with c and stays constantly equal to the total density ρ in the fluid state.

Numerical results confirm the theoretical prediction in Table 2.1 on the phase diagram of the model: fluid state for $\rho < c$ and condensed state for $\rho > c$. The phase diagram can be justified intuitively imagining to prepare the system in the fluid state and trying to guess the consequent evolution. Indeed, the behavior for $\rho > \max\{T, c\}$ is rather intuitive: initially the typical number of particles at each site would be above the threshold and particles would leave the defect site at rate c and the regular sites at rate $\rho > c$, so that eventually the system would reach the condensed state. The behavior in the case $\rho < \min\{T, c\}$ is somehow opposite: in the fluid state the typical number ρ of particles at each site would be smaller than T and c. Particles would leave each site of the lattice with rate ρ and the system would remain in the fluid state. The case $T < \rho < c$ is more subtle: particles would leave the defect

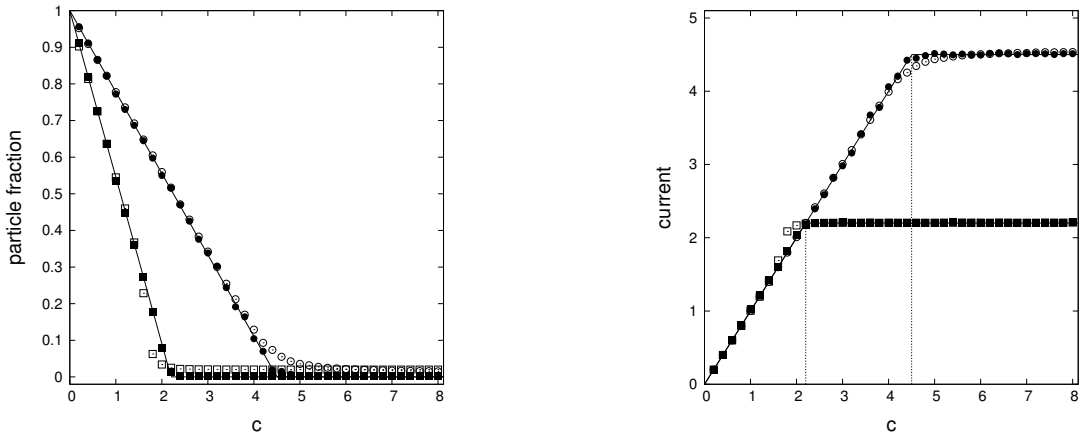

Figure 2.4: Particle fraction at the defect site (left panel) and stationary current (right panel) vs. the saturated rate c. Open and solid symbols are the Monte Carlo prediction for $L = 50$ and $L = 500$, respectively. The forward hopping probability is $p = 1$. Circles and squares refer, respectively, to $T = 3$ and $\rho = 4.5$ ($\circ$ and $\bullet$) and $T = 7$ and $\rho = 2.2$ ($\square$ and $\blacksquare$). Solid lines are the theoretical predictions in Table 2.1, whereas the dotted lines indicate, respectively, the values of the saturated rate $c = 2.2$ and $c = 4.5$.

site at rate c and the regular sites at rate $\rho < c$. The rate limitation at the defect site is not effective and the system remains in the fluid state. The case $c < \rho < T$ is the most interesting one: since $\rho < T$, in the fluid state each site is initially left by particles at the same rate ρ. But if a random fluctuation increased the number of particles at the defect site to a value larger than T, particles would then start to leave such a site at a rate smaller than ρ (the rate at which particles leave the regular sites in the fluid state), which would thus induce the transition to the condensed state. Being T finite, we expect that the probability for such a fluctuation is so large to justify that the stationary state is the condensed one.

3. Analytical solution

The model will be studied by using techniques similar to those developed in [26, Section 5.2] and [12]. We first recall the expression

$$J_{L,N} = (2p-1)\frac{Z_{L,N-1}}{Z_{L,N}} \tag{3.4}$$

for the current proven in [26, equation (11)]. Thus, our strategy will be the following: we shall first compute the partition function $Z_{L,N}$ and use (3.4) to deduce the current. Then, exploiting (2.3) and the definition of the updating rates at the regular sites, we shall compute

$$m_{x,L,N} = \frac{1}{2p-1}\, J_{L,N} \tag{3.5}$$

for $x = 2, \dots, L$. Finally, the trivial equality,

$$m_{1,L,N} = N - (L-1)m_{x,L,N} \tag{3.6}$$

with x any site different from the defect one, will provide

$$\nu = 1 - \frac{1}{\rho}\, m_{x,L,N} \quad . \tag{3.7}$$

Simple algebra and the use of the multinomial theorem, see, e.g. [31, equation (3.35)] allow to rewrite the partition function (2.2) as

$$Z_{L,N} = Z^{(1)}_{L,N} + Z^{(2)}_{L,N} \tag{3.8}$$

with

$$Z^{(1)}_{L,N} = \sum_{k=0}^{T} \frac{1}{k!(N-k)!}(L-1)^{N-k} \tag{3.9}$$

and

$$Z^{(2)}_{L,N} = \frac{c^T}{T!} \sum_{k=T+1}^{N} \frac{1}{c^k (N-k)!}(L-1)^{N-k} \tag{3.10}$$

In $Z^{(1)}_{L,N}$ the sum extends to the finite value T, thus the factorial can be approximated as

$$(N-k)! = \frac{N!}{N(N-1)\cdots(N-k+1)} \approx \frac{N!}{N^k} \tag{3.11}$$

yielding

$$Z^{(1)}_{L,N} \approx \frac{(L-1)^N}{N!} \sum_{k=0}^{T} \frac{1}{k!}\, \rho^k \tag{3.12}$$

The estimate of the sum in (3.10) is more delicate since the index k can be arbitrarily large when the thermodynamic limit is considered. To evaluate the behavior of the partition function in the above limit, it is useful to introduce the function $I(k)$ by rewriting (3.10) as $Z^{(2)}_{L,N} = \sum_{k=0}^{N} \exp\{LI(k)\}$. To understand where the maxima of $I(k)$ are located, we express $I(k+1) - I(k)$ as

$$I(k+1) - I(k) = \frac{1}{L} \log \frac{N-k}{c(L-1)} \quad ,$$

which implies that $I(k+1) - I(k) > 0$ if and only if $k < N - c(L-1)$. Hence, for $\rho < c$ the function $I(k)$ attains its maximum value at $k = T+1$, whereas for $\rho > c$ the maximum is at $k^* = \lfloor (\rho - c)L \rfloor$.

Case $\rho < c$. The sum (3.10) is dominated by the first terms, hence, recall T is finite, the factorial can be treated as in (3.11). Thus,

$$Z^{(2)}_{L,N} \approx \frac{c^T}{T!}\, \frac{(L-1)^N}{N!} \sum_{k=T+1}^{N} \left(\frac{\rho}{c}\right)^k$$

Performing the change of variables $h = k - (T+1)$ and extending the sum up to infinity we find

$$Z^{(2)}_{L,N} \approx \frac{\rho^T}{T!} \frac{(L-1)^N}{N!} \frac{\rho/c}{1-\rho/c} \quad . \tag{3.13}$$

Finally, using (3.4), (3.12), and (3.13) we get $J = (2p-1)\rho$. Moreover, (3.5) and (3.6) yield $m_x = \rho$ for any $x = 1, \dots, L$.

Case $\rho > c$. The sum (3.10) is dominated by the terms in an interval centered at $k^* = \lfloor (\rho - c)L \rfloor$. The factorial in (3.10) can be approximated using the Stirling formula; setting $x = k/L$ we have

$$\frac{1}{c^k (N-k)!} (L-1)^{N-k} = \frac{1}{\sqrt{2\pi L(\rho - c)}} e^{LF(x)}$$

with

$$F(x) = (\rho - x) - x \log c - (\rho - x) \log(\rho - x) \quad .$$

Hence, the sum in (3.10) can be approximated as the following integral

$$Z^{(2)}_{L,N} = \frac{c^T}{T!} \sqrt{\frac{L}{2\pi}} \int_{(T+1)/L}^{\rho} \frac{1}{\sqrt{\rho - x}} \, e^{LF(x)} \, \mathrm{d}x$$

The function $F(x)$ has obviously a maximum at $x^* = \rho - c$. We can expand the exponent in Taylor series up to the second order and compute the Gaussian integral to get

$$Z^{(2)}_{L,N} \approx \frac{c^T}{T!} \frac{1}{\sqrt{c}} e^{Lc - N \log c} \quad . \tag{3.14}$$

To compare (3.14) and (3.12), we use the Stirling approximation to write $(L-1)^N/N! \approx \exp\{N - N \log \rho\}/\sqrt{2\pi N}$. Since, $Lc - N \log c > N - N \log \rho$, we have that

$$Z_{L,N} \approx \frac{c^T}{T!} \frac{1}{\sqrt{c}} e^{Lc - L \log c} \left(1 + \frac{Z^{(1)}_{L,N}}{Z^{(2)}_{L,N}} \right) \tag{3.15}$$

with $Z^{(1)}_{L,N} / Z^{(2)}_{L,N} \to 0$ in the thermodynamic limit.

Finally, using (3.4) and (3.15) we get $J = (2p-1)c$. Moreover, (3.5) and (3.7) yield $m_x = c$ for any $x = 2, \dots, L$ and $\nu = (\rho - c)/\rho$.

4. Discussion

We discuss our results in view of the pedestrian flow interpretation proposed in Section 1 (see also Fig. 1.1), sticking to the case $p = 1$.

From the point of view of pedestrian flows, in the ZRP model each regular site is left by a walker at rate equal to the number of people which are at that time at the site. This means that in a time of order one all the people at the site will abandon it, hence, the local current is equal to the occupation number of the cell. For the same reason, if the defect site occupation number is small (smaller than the saturation threshold), the outgoing current is equal to the defect cell occupation number as well. On the other hand, if the defect site occupation number is large, the number of walkers leaving such a site in a unit of time is equal to the constant value c (the saturated rate) and hence the local current is equal to c.

Thus, in case the total density ρ is smaller than c, one can guess that the stationary state has the walkers distributed uniformly at the sites of the lattice. Indeed, at each site the local current would be equal to ρ. This is the *fluid state*. On the other hand, if $\rho > c$, it can happen that, at a certain time, a bunch of people larger than the saturation threshold reaches simultaneously the defect cell. This would reduce, on that site, the local current to c, giving then rise to a stationary state characterized by an accumulation of walkers at the blocked site and a stationary current equal to c. This is what we call *condensed* or *trapping state*. This is a remarkable phenomenon. Indeed, even in the case in which the capacity reduction becomes effective at the defect site only above a certain saturation threshold larger than the saturation rate (note that we can compare these two quantities since the particle speed away from the bottleneck is one), provided $\rho > c$, the "jammed" state can be induced by a local fluctuation larger than the saturation threshold, even if the total density ρ is smaller than the activation threshold T.

Imagine c to be proportional to the width of a door or corridor disturbing the pedestrian flow. Then the capacity reduction affects the pedestrian rate. Essentially, the pedestrian flow appears to increase proportionally to the width of the door as observed in the experiments in [2, 3].

A relevant question about pedestrians flow in presence of bottlenecks is that of understanding the dependence of the pedestrian speed on the local density, namely, the so called *fundamental diagram*. We shall define the local speed of the particles as the ratio between the stationary current and the stationary occupation number. Since, away from the defect site, the current and the stationary occupation number are equal (see the results in Table 2.1 for $p = 1$), the walkers speed is one independently of the number of walkers at the site. This is quite obvious for our version of the ZRP model, since excepted for the defect site the site updating rate is proportional to the occupation number.

At the defect site we have to distinguish between the fluid and the condensed state. In the former, see Table 2.1 for $p = 1$, the speed is one, whereas in the latter it is c/m_1 (note we are considering a large volume situation, but we are not considering the thermodynamic limit,

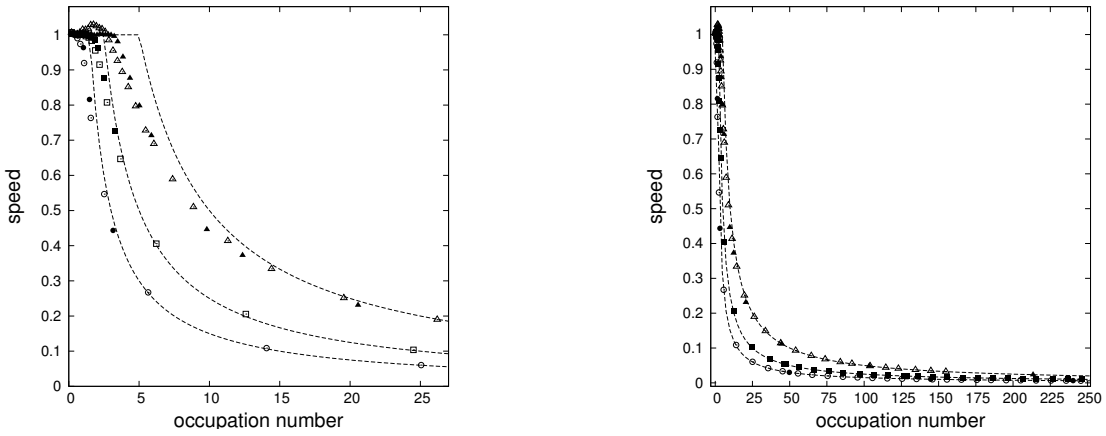

Figure 4.5: Speed (stationary current divided times the stationary occupation number) at the defect site vs. the stationary occupation number at the same site. Open and solid symbols are the Monte Carlo prediction for $L = 50$ and $L = 500$, respectively. All simulations refer to the case $p = 1$. Triangles refer to the case $T = 3$ and $c = 5$ with ρ ranging from 0.2 to 6.0. Squares refer to the case $T = 6$ and $c = 2.5$ with ρ ranging from 0.2 to 3.5. Circles refer to the case $T = 4$ and $c = 1.5$ with ρ ranging from 0.2 to 2.5. The dashed lines are the theoretical prediction: the speed is 1 in the fluid phase and c/m_1 in the condensed phase, which correspond in the picture to the regions $m_1 < c$ and $m_1 > c$, respectively. The left panel is a magnification of the right panel for low values of the stationary occupation number at the defect site.

indeed, m_1 would diverge in the condensed state). In other words, since in the condensed state the current is constant at the defect site, we have that there the local speed decreases as the inverse of the mean occupation number. This behavior is observed experimentally in [30, Figure 4], where the authors perform an experiment with walkers moving on a lane and forced to pass through a corridor with reduced width with respect to the main lane. The authors measure the speed of the pedestrians at the bottleneck as a function of their density at the same spot. They find precisely the same behavior we report in Fig. 4.5 for $c = 1.5$.

Figure 4.5 is obtained by plotting the stationary speed at the defect site as a function of the stationary occupation number at the same site. Each curve in the plot is obtained for a fixed value of the saturated rate c. We consider the cases $c = 1.5, 2.5, 5$ (see the figure caption for more details). For each value of c, we obtain the different stationary states plotted in the graph (circles, squares, and triangles), by varying the total density ρ. According to the results in Table 2.1, in this way we obtain fluid stationary states with $m_1 = \rho$ for ρ smaller that c and condensed states with $m_1 = (\rho - c)L + c$ for ρ larger than c. The dashed lines represent the theoretical prediction: speed equal to 1 in the fluid state and to c/m_1 in the condensed one. As for the simulations discussed in figures 2.2–2.4 the match between the theoretical and the Monte Carlo results is strikingly good.

It is important to remark that our results for $c = 1.5$ reproduce with high accuracy the experimental behavior illustrated in [30, Fig. 4 left–top panels] for large local densities. We use the value $c = 1.5$ since in [30, Fig. 4 left–bottom panels] it is shown that in this density regime the current is approximatively equal to 1.5. This value for c can be also guessed by looking at the picture of the experimental setup shown in [30, Fig. 2]. Indeed the corridor is so narrow that walkers can pass through one or two at a time. Since our model predicts very well the experimental behavior, we conclude that the structure of the experimental fundamental diagram is essentially due to the fact that the stationary current in the corridor does not depend on the number of pedestrians approaching it. At low local densities, experimental results depart from the inverse proportionality behavior with respect to the local densities, but the abrupt onset of the constant behavior we find in our model is not observed. This is quite natural, since in our model the threshold effect is sharp, whereas we expect that in crowd evacuation experiments the capacity reduction becomes effective in a sort of mild, continuous fashion.

It is also worth mentioning that in [35] pedestrian fundamental diagrams are studied in the framework of a social force model with an hard core parameter reflecting the size of the pedestrians. The fundamental diagram in [35, Figures 1–2] share some similarities with those displayed here in Fig. 4.5, although the setup is completely different; in particular, no bottleneck mechanism is included in their model. Yet, the diagrams show the same saturation effect occurring at low densities, meaning that in that regime pedestrians move freely with their own velocity and are not influenced by other walkers.

Results related to the ones discussed in this paper can be also found in [37], where the authors study numerically a two–dimensional lattice model, similar to the one considered in [14], in which particles perform a biased random walk in a square with an exclusion rule. Particles preferentially move to the right and a sort of bottleneck constrains the flow in the middle of the lattice. The current is measured as a function of the rate at which particles enter the left boundary and profiles similar to those that we plotted in figures 2.3 and 2.4 (right panel) are found. In other words, their two–dimensional model shows a behavior similar to the one we proved for our one–dimensional case: the onset of a sort of condensed stationary state, induced by a large left boundary entry rate, is observed numerically and in such a state the pedestrian current becomes constant.

We finally remark that by letting the threshold scale with L, our model gives rise, in the thermodynamic limit, to fluid states only. The trapping state is indeed prevented by the absence of large enough fluctuations in the number of particles at the bottleneck (pedestrian density waves [38]).

References

[1] B.S. Kerner, H. Rehborn, Experimental properties of complexity in traffic flow. *Physical Review E* **53**, R4275 (1996).

[2] S. Yamamoto, Y. Hieida, S. Tadaki, Effects of Bottlenecks on Veichle Traffic. *Journal of the Physical Society of Japan* **75**, 114601 (2006).

[3] T. Kretz, A. Grünebohm, M. Schreckengerg, Experimental study of pedestrian flow through a bottleneck. *Journal of Statistical Mechanics: Theory and Experiment* **10**, 10014 (2006)

[4] W. Liao, A. Seyfried, J. Zhang, M. Boltes, X. Zheng, Y. Zhao, Experimental study on pedestrian flow through wide bottleneck. *Transportation Research Procedia* **2**, 26–33 (2014).

[5] D. Helbing, M. Isobe, T. Nagatani, K. Takimoto, Lattice gas simulation of experimentally studied evacuation dynamics. *Physical Review E* **67**, 067101 (2003)

[6] W. Daamen, S. Hoogendoorn, Capacity of Doors during Evacuation Conditions. *Procedia Engineering* **3**, 53–66 (2010).

[7] N. Bellomo, A. Bellouquid, D. Knopoff, From the macroscale to collective crowd dynamics. *Multiscale Modelling and Simulation* **11**, 943–963 (2013).

[8] N. Bellomo, J. Soler, On the mathematical theory of the dynamics of swarms viewed as complex systems. *Math. Models Methods Appl. Sci.* **22**, 1140006 (2012).

[9] N. Bellomo and S.–Y. Ha, A quest toward a mathematical theory of the dynamics of swarms. *Math. Models Methods Appl. Sci.* **27**, 745–770 (2017).

[10] B. Mishra, D. Chowdhury, Interference of two co–directional exclusion processes in the presence of a static bottleneck: a biologically motivated model. Preprint arXiv: 1703.07333v1.

[11] S.A. Janowsky, J.L. Lebowitz, Exact Results for the Asymmetric Simple Exclusion Process with a Blockage. *J. Stat. Phys.* **77**, 35–51 (1994).

[12] E.N.M. Cirillo, M. Colangeli, A. Muntean, Blockage induced condensation controlled by a local reaction. *Physical Review E* **94**, 042116 (2016).

[13] B. Scoppola, C. Lancia, R. Mariani, On the Blockage Problem and the Non–analiticity of the Current for Parallel TASEP on a Ring. *J. Stat. Phys.* **161**, 843–858 (2015).

[14] E.N.M. Cirillo, A. Muntean, O. Krehel, R. van Santen, A lattice model of reduced jamming by barrier. *Physical Review E* **94**, 042115 (2016).

[15] E.N.M. Cirillo, A. Muntean, O. Krehel, R. van Santen, A. Sengar, Residence time estimates for asymmetric simple exclusion dynamics on strips. *Physica A* **442**, 436–457 (2016).

[16] B.E. Fitzgerald, J.T. Padding, R. Van Santen, Simple diffusion hopping model with convection. *Physical Review E* **95**, 013307 (2017).

[17] E. Ronchi, E.D. Kuligowski, D. Nilsson, R.D. Peacock, P.A. Reneke, Assessing the verification and validation of building fire evacuation models. *Fire Technology* **52**, 197–219 (2016).

[18] M. Moussaïd, M. Kapadia, T. Thrash, R.W. Sumner, M. Gross, D. Helbing, C. Hölscher, Crowd behaviour during high–stress evacuations in an immersive virtual environment. *J. R. Soc. Interface* **13**, 20160414 (2016).

[19] E.N.M. Cirillo, M. Colangeli, A. Muntean, Does communication enhance pedestrians transport in the dark? *Comptes Rendus Mecanique* **344**, 19–23 (2016).

[20] E.N.M. Cirillo, M. Colangeli, A. Muntean, Effects of communication efficiency and exit capacity on fundamental diagrams for pedestrian motion in an obscure tunnel – a particle system approach. *Multiscale Model. Simul.* **14**, 906–922 (2016).

[21] O. Hirschberg, D. Mukamel, G.M. Schütz, Condensation in Temporally Correlated Zero-Range Dynamics. *Phys. Rev. Lett.* **103**, 090602 (2009).

[22] O. Hirschberg, D. Mukamel, G.M. Schütz, Motion of condensates in non-Markovian zero-range dynamics. *J. Stat. Mech. Theory Exp.* P08014 (2012).

[23] M. Cavallaro, R.J. Mondragón, R.J. Harris, Temporally correlated zero–range process with open boundaries: Steady state and fluctuations. *Phys. Rev. E* **92**, 022137 (2015).

[24] J. Kaupužs, R. Mahnke, R.J. Harris, Zero-range model of traffic flow. *Phys. Rev. E* **72**, 056125 (2005).

[25] M.R. Evans, Phase Transitions in One–Dimensional Nonequilibium Systems *Brazilian Journal of Physics* **30**, 42–57 (2000).

[26] M.R. Evans, T. Hanney, Nonequilibrium statistical mechanics of the zero–range process and related models. *J. Phys. A: Math. Gen.* **38**, R195–R240 (2005).

[27] C. Godréche, J.M. Luck, Condensation in the inhomogeneous zero–range process: an interplay between interaction and diffusion disorder. *J. Stat. Mech.: Theory and Experiment*, P12012 (2012).

[28] P. Chleboun, S. Grosskinsky, A dynamical transition and metastability in a size–dependent zero–range process. *J. Phys. A: Math. Theor.* **48**, 055001 (12pp) (2015).

[29] S. Grosskinsky, G.M. Schütz, Discontinuous Condensation Transition and Nonequivalence of Ensembles in a Zero–Range Process. *J. Stat. Phys.* **132**, 77–108 (2008).

[30] W. Daamen, S.P. Hoogendoorn, Frist–order Pedestrian Traffic Flow Theory. *Transportation Research Board Annual Meeting*, 1–14 (2005).

[31] R. Nelson, *Probability, Stochastic Processes, and Queueing Theory. The Mathematics of Computer Performance Modeling*, Springer Verlag, New York (1995).

[32] M.E.J. Newman and G.T. Barkema, *Monte Carlo Methods in Statistical Physics.* Clarendon Press, Oxford, UK, 1999.

[33] L. Pareschi, G. Toscani, *Interacting Multiagent Systems: Kinetic Equations and Monte Carlo Methods.* Oxford University Press, Oxford, UK, 2013.

[34] P. Barbante, A. Frezzotti, L. Gibelli, A kinetic theory description of liquid menisci at the microscale. *Kinet. Relat. Mod.* **8**, 235–254 (2015).

[35] A. Seyfried, B. Steffen, T. Lippert, Basics of modelling the pedestrian flow. *Physica A* **386**, 232–238 (2006).

[36] T. Nagatani, Dynamica transition and scaling in a mean–field model of pedestrain flow at a bottleneck. *Physica A* **300**, 558–566 (2001).

[37] Y. Tajima, K. Takimoto, T. Nagatani, Scaling of pedestrian channel flow with a bottleneck. *Physica A* **294**. 257–268 (2001).

[38] A. Schadschneider, W. Klingsch, H. Klüpfel, T. Kretz, C. Rogsch, A. Seyfried, Evacuation Dynamics: Empirical Results, Modeling and Applications. Encyclopedia of Complexity and Systems Science, pp. 3142–3176, Springer New York, 2009.